Journal of Sound and Vibration 625 (2026) 119604

Contents lists available at ScienceDirect

Journal of Sound and Vibration

journal homepage: www.elsevier.com/locate/jsvi

Quantification of structural damage by harnessing the principle of local force continuity

Yuting Yang [a,b], Yu'e Ma [b,*], Linfeng Li [a], Li Cheng [a,*], Xiang Yu [a,*]

[a] Department of Mechanical Engineering, The Hong Kong Polytechnic University, Hung Hom, Kowloon, Hong Kong SAR
[b] National Key Laboratory of Strength and Structural Integrity, School of Aeronautics, Northwestern Polytechnical University, Xi'an, China

ARTICLE INFO

Keywords:
Damage quantification
Vibration response
Local continuity
Structural health monitoring

ABSTRACT

Quantitative assessment of damage severity is important for maintaining and extending the service life of engineering structures. Traditional vibration-based methods often face challenges such as low sensitivity, strong dependence on structural details and excitation signals, and the need for global models or baseline signals. The recently developed Pseudo Excitation (PE) method enables the detection of local structural damage by utilizing high-order spatial derivatives of the measured displacement data, easing some of these constraints. However, the PE method can only pinpoint the presence of damage and outline its boundaries; it currently lacks the ability to quantify the damage severity or the profile of the damaged area. To address these limitations, this study proposes a novel damage quantification approach, referred to as Local Force Continuity (LFC) method, based on the continuity principle of local internal forces. By examining the force continuity relations near the damage boundary, we establish a correlation between the damage severity and the measured vibration responses, enabling a quantitative characterization of the damage profile. The proposed approach is first validated through numerical simulations, showcasing its remarkable ability in locating damage and identifying its shape. The effects of damage extents, excitation frequency and structural boundary conditions are systematically investigated, highlighting the effectiveness and robustness of the proposed method. Finally, experimental verification is conducted using laser doppler vibrometer (LDV) scanning. Results demonstrate that the LFC method can effectively assess damage severity. The LFC method not only retains the advantages of the PE method, but also significantly extends its capabilities in damage quantification, providing new physical insights and broadening its potential applications in related engineering fields.

1. Introduction

Safety of engineering structures is of paramount importance, necessitating stringent standards for reliability, integrity, and durability [1–3]. To monitor structural conditions, extensive research has led to the development of various non-destructive testing (NDT) techniques based on different physical principles, encompassing a diverse range of technologies including ultrasonic inspection [4], shearography [5], magnetic resonance imagery [6], laser interferometry [7], acoustic emission [8], etc. Among them, vibration-based methods have garnered significant attention due to their cost-effectiveness, ease of implementation, and potential for

* Corresponding authors.
E-mail addresses: ma.yu.e@nwpu.edu.cn (Y. Ma), li.cheng@polyu.edu.hk (L. Cheng), lucien.yu@polyu.edu.hk (X. Yu).

https://doi.org/10.1016/j.jsv.2025.119604
Received 20 March 2025; Received in revised form 30 November 2025; Accepted 8 December 2025
Available online 9 December 2025

real-time structural health monitoring in complex structures [9–12].

The fundamental principle underlying vibration-based detection methods is that the presence of damage, such as notches or cracks, alters the physical parameters of the structure (exemplified by stiffness and mass distribution and damping) compared to the baseline values obtained in the pristine structure. These variations can lead to changes in the vibration response, including eigenfrequencies [13], mode shapes [14], and their derivatives [15] etc. Among them, natural frequencies reflect alterations in the global vibration characteristics of the structure, which can be obtained from the frequency response functions. However, they primarily indicate the presence of severe damage, as global parameters cannot provide detailed information about the damage's location and shape [16]. In contrast, changes in mode shapes, which inherently contain spatial information about the structural dynamics, can more effectively inform on the location and extent of damage. Nonetheless, measuring mode shapes requires sophisticated experimental setups, and the damaged-induced changes may be subtle and challenging to detect [17]. Consequently, researchers have turned to examine the higher-order derivatives of the structural displacement (mode shapes or *in-situ* deflection shape) to assess the location and severity of damage [18,19], with demonstrated applicability. For example, Chang et al. [20] defined a damage indicator based on the first derivative of mode shapes, referred to as rotational modes. Alternatively, damage index was also defined in terms of curvature or strain energy [21], or shear force or vibrational power flow [22], which involve the second and the third derivative with respect to structural displacement, respectively. For force identification problems, the fourth derivative was also deployed [21]. Compared to mode shape methods, the derivative-based approach does offer greater sensitivity and higher detection accuracy. However, noises in the measurement are omni-present and unavoidable, thus drastically affecting the accuracy of the higher-order derivative operation. Overall, conventional physics-based techniques still face several common limitations, including relatively limited precision in detecting minor damages, the need for baseline signals and global models, and difficulties in identifying damage within complex structures.

To address these challenges, emerging techniques such as signal processing and machine learning have attracted significant attention in recent years [22–24]. Advanced signal processing techniques, such as Hilbert Transform, can efficiently extract and analyze critical information from complex vibration signals based on dedicate formulations and algorithms [25]. Meanwhile, machine learning techniques offer powerful capabilities in pattern recognition and automatic feature extraction from abundant history data. Despite the promise offered by these techniques [26,27], they still suffer from poor result interpretability due to the lack of a solid physical foundation and venerable sensitivity to modeling or measurement errors. Thus, they have not fully addressed the inherent limitations of traditional vibration-based damage detection methods.

To overcome these constraints, Pseudo Excitation (PE) approach was developed over the past decade to identify structural damages by examining the local dynamic equilibrium based on high-order spatial derivatives of the displacement field [28]. The fundamental principle of the PE approach is that the presence of damage would disrupt the original local dynamic equilibrium of the healthy structure, thus allowing the use of a Damage Index (DI) to describe the "pseudo force" generated by the damage and its location. Unlike conventional global vibration-based methods, the PE approach leverages the local examination of specific components in a structure, which can be complex and difficult to model, to achieve accurate detection and localization of the damage. Initially, a strong form of the DI was developed, with demonstrated success in localizing damage across various engineering structures, including beams [29], plates [30], reinforced concrete structures [31], honeycomb sandwich structures [32], laminated composites [33], cables [34], and cylinders [35] etc. To further enhance this efficacy, particularly in terms of getting increased robustness against noise and reducing measurement points required for higher-order derivative estimation, a weak form PE formulation was proposed [36], by utilizing weighted integration of interval damage indicators, thus enabling a paradigm shift from pointwise detection to regional detection. On this basis, methods such as the virtual vibration displacement method and the sparse boundary measurement method were proposed, thus enabling online structural health monitoring [37].

Despite the encouraging progress, different versions of the PE approach currently fail to quantitively assess the damage severity. This limitation hinders its practical application, where accurate and detailed damage assessment is crucial for informed decision-making and the development of effective repair strategies. To address this issue, this study proposes a novel damage quantification approach based on the continuity relation of local internal forces, which are intrinsically linked to the flexural stiffness and spatial derivatives of vibration displacements. The fundamental principle underpinning this approach is that when damage presents, structural flexural stiffness undergoes changes; yet the local internal forces, even near the damaged areas, remain continuous. As a result, spatial derivatives of the displacement field can be utilized to quantify changes in flexural stiffness. If flexural stiffness can be explicitly defined by the structure's cross-section and material properties, the damage severity related to the change in the cross-section can be quantified inversely. The proposed method retains all the advantages of local vibration-based detection methods, such as eliminating the need for baseline signals and global structural models, and not being constrained by a specific excitation frequency, making it well-suited for complex structures. Furthermore, the proposed method enhances the capability of the PE method for damage quantification by incorporating lower-order displacement derivatives, thereby enhancing the robustness of the process of damage identification. These appealing features open new avenues for developing a practical SHM technique that can provide abundant damage-specific information in complex systems.

This paper is organized as follows: Section 2 introduces the principle of the proposed LFC approach. Section 3 validates the approach through numerical simulations, examining quantification accuracy across key parameters including frequency selection, damage location, and boundary conditions. Section 4 validates the approach experimentally using Laser Doppler Vibrometer (LDV) measurements on damaged beam specimens. Conclusions are given in the last section.

2. Local force continuity (LFC)

The proposed LFC approach essentially formulates the problem of damage identification by quantitively assessing the local force

continuity relation. When a structure vibrates under external harmonic excitation, only internal forces are present at locations away from the excitation source. This ensures that the spatial derivatives of the vibration displacement field and the internal forces inherently satisfy a specific equilibrium relationship. As a result, variations in physical parameters, such as bending strength, modulus or cross-section, can be inferred by analyzing changes in the derivatives of vibration field. This section elaborates on the theoretical background of the proposed LFC approach.

2.1. Dynamic response of a general elastic structure

Consider a general three-dimensional elastic structure represented by domain $\boldsymbol{\Omega}$ as shown in Fig. 1, containing a damaged region denoted as $\boldsymbol{\Omega}_d$. The structure is subjected to a harmonic external excitation force, $\mathbf{f}(\mathbf{x},t)$, which induces vibrations in the elastic body.

Assuming that nonlinear effect in the system can be neglected and that the vibration amplitude in the elastic body is small, the displacement field $\mathbf{u}(\mathbf{x},t)$ at any point within the domain $\boldsymbol{\Omega}$ (where the position vector $\mathbf{x} \in \boldsymbol{\Omega}$) can be obtained by solving the governing equation in its strong form:

$$\nabla \cdot \boldsymbol{\sigma}(\mathbf{u}) + \mathbf{g}(\mathbf{x},\mathbf{t}) + \rho\ddot{\mathbf{u}} = 0 \tag{1}$$

where $\mathbf{g}(\mathbf{x},t)$ represents the body forces. The above equation can be solved by applying the appropriate boundary conditions. On the displacement boundary, we have

$$\mathbf{u}(\mathbf{x},t) = \mathbf{u}_0(\mathbf{x},t) \tag{2}$$

On the force boundary,

$$\boldsymbol{\sigma}(\mathbf{u}) \cdot \mathbf{n} = \mathbf{f}(\mathbf{x},t) \tag{3}$$

where ρ is density; $\mathbf{n}$ represents the normal vector to the force boundary; $\boldsymbol{\sigma}(\mathbf{u})$ is stress tensor, which is the product of elasticity tensor $\mathbf{C}$ and the strain tensor $\boldsymbol{\varepsilon}(\mathbf{u})$, expressed as

$$\boldsymbol{\sigma}(\mathbf{u}) = \mathbf{C} : \boldsymbol{\varepsilon}(\mathbf{u}) \tag{4}$$

$$\boldsymbol{\varepsilon}(\mathbf{u}) = \frac{1}{2}\left\{\nabla\mathbf{u} + (\nabla\mathbf{u})^T\right\} \tag{5}$$

where ":" denotes a double dot product. Assuming the structure undergoes steady-state vibration, the displacement field can be transferred to the frequency domain as:

$$\mathbf{u}(\mathbf{x},t) = \mathbf{U}(\mathbf{x},\omega)e^{j\omega t} \tag{6}$$

where ω is the angular frequency of the external force. In this study, only time-invariant body forces are considered, and among these, self-weight is the only body force included in the analysis. Like other time-invariant body forces, self-weight manifests as a constant offset in the time domain and is typically excluded from frequency domain analysis. Consequently, in the free section where $\boldsymbol{\Omega}$ is not constrained by displacement or force boundaries, substituting Eq. (6) into Eq. (1) yields

$$\nabla \cdot \boldsymbol{\sigma}(\mathbf{U}) - \omega^2\rho\mathbf{U} = 0 \tag{7}$$

This paper focuses on dynamic responses such that the omission of the body force term will not affect the method's accuracy. The steady-state response can be obtained by solving Eq. (7) under specified boundary conditions. Equations (1)-(7) depict the forward solution procedure for solving the vibration response of the elastic body. Equation (7) can be made more complete by adding the

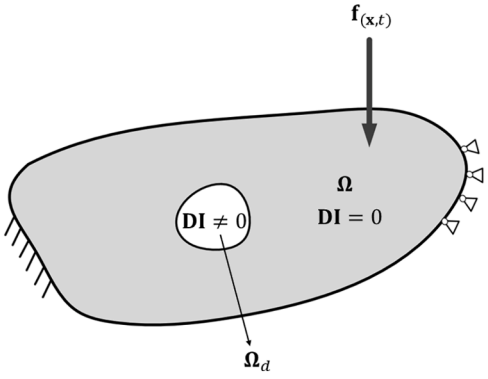

Fig. 1. Three-dimensional elastic domain with damage.

harmonic excitation force:

$$\nabla \cdot \boldsymbol{\sigma}(\mathbf{U}) - \omega^2 \rho \mathbf{U} = \mathbf{L}\mathbf{U} = \mathbf{F}\delta(\mathbf{x} - x_e) \tag{8}$$

where **L** refers to matrix differential operator, **U** is the displacement field, **F** represents external forces applied at position x_e, and δ is Dirac function, which is equal to 1 when $x = x_e$ and 0 for all other values of x.

In conventional vibration-based damage detection methods, analyzing the global responses such as natural frequencies, mode shape functions, or frequency response functions—can, in principle, indicate whether a structure contains damage by comparing measured vibration responses with simulated ones or the baseline signals. However, their efficiency and accuracy are heavily dependent on the fidelity of the global model and the solution process, which are also easily affected by the change of boundary conditions and excitation signals.

2.2. Pseudo excitation (PE) method and damage index (DI)

PE approach capitalizes on the local examination of the dynamic equilibrium conditions of a structural component using high-order spatial derivatives of displacement data. For the same elastic body containing a damaged region as illustrated in Fig. 1, its free section excluding any external excitation forces can be formulated as:

$$\mathbf{DI} = \nabla \cdot \boldsymbol{\sigma}(\mathbf{U}) - \omega^2 \rho \mathbf{U} = \mathbf{L}\mathbf{U} = 0 \tag{9}$$

where the elastic force and the inertia force are balanced locally at any point within the structure. The occurrence of damage would lead to changes in the structural parameters, resulting in a violation of Eq. (9) and indicating a disruption of the original equilibrium condition, as illustrated in Fig. 1. **DI** = **LU** in Eq. (9) is thus defined in the PE approach as a Damage Index (DI) to signal whether structural damage occurs at the examined point.

In general, PE approach is applicable to both simple structural components such as beams, plates, and shells, and complex systems involving their combinations. The only prerequisite is that the local equilibrium relationship in the elastic body can be explicitly formulated. In the simplest case of a homogeneous isotropic Euler-Bernoulli beam element, DI can be explicitly defined as

$$\mathrm{DI} = E_0 I_0 \frac{d^4 w(x)}{dx^4} - \rho_0 A_0 \omega^2 w(x) \tag{10}$$

where $w(x)$ refers to the transverse displacement of the beam element at any point x, E_0, I_0, ρ_0, and A_0 are the Young's modulus (complex number if material damping is considered), density, moment of inertia and cross-section area of the intact region of the beam; respectively. In the damaged region, assuming that damage causes a reduction in the mass and stiffness as compared to the healthy status, $\Delta_{\rho A}$ and Δ_{EI}, respectively, the above equation can be re-written as

$$(E_0 I_0 - \Delta_{EI}) \frac{d^4 w(x)}{dx^4} - (\rho_0 A_0 - \Delta_{\rho A}) \omega^2 w(x) = 0 \tag{11}$$

where DI can be explicitly determined as:

$$\mathrm{DI} = E_0 I_0 \frac{d^4 w(x)}{dx^4} - \rho_0 A_0 \omega^2 w(x) = \Delta_{EI} \frac{d^4 w(x)}{dx^4} - \Delta_{\rho A} \omega^2 w(x) \tag{12}$$

It is clear that a non-zero value of DI indicates the presence of structural damage, underscoring the fundamental principle of the PE approach. In previous research, the PE approach has demonstrated remarkable ability for damage localization [28,32,34]. Specifically, the PE method's local formulation ensures exceptional immunity to perturbations in structural boundary conditions and excitation frequencies. However, the lack of ability to quantitatively assess the damage severity remains a bottlenecking issue.

2.3. Damage quantification using LFC

To revamp and improve the PE approach from damage localization to quantification, we introduce a method based on the principle of local force continuity. Using the Euler-Bernoulli beam as a simple example, Fig. 2 illustrates a damaged beam with a damaged region from x_i to x_j, represented by a slot with a depth of a. We first assume that no external forces exist near the damage, and the changes in the bending stiffness are solely due to damage. In regions distant from external forces, the principle of force transmissibility and continuity ensures that internal forces within a structure remain continuous at any point without sudden changes.

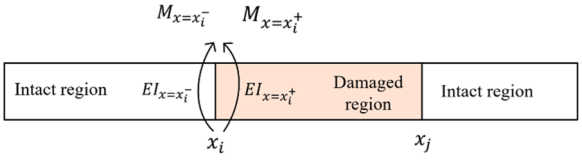

Fig. 2. Local internal force continuity in a beam structure containing a damaged region.

Consequently, within an infinitesimal volume element, internal force variations exhibit smooth and continuous behavior without discontinuities. Therefore, at the left boundary x_i of the damaged area, the bending moments (as internal forces) on the left and right sides of this interface, $M_{x=x_i^-}$ and $M_{x=x_i^+}$, respectively, are equal, which can be expressed as:

$$M_{x=x_i^-} = M_{x=x_i^+} = M \tag{13}$$

where the subscript $x = x_i^-$ and $x = x_i^+$ represent the corresponding physic quantities on the left and right of x_i, respectively. The bending moment can be calculated by the product of flexural stiffness and deflection curvature as:

$$M = EI\frac{d^2w}{dx^2} \tag{14}$$

On the two sides across the damage boundary, the left-hand side maintains their integrity with an intact bending stiffness referred to as $EI_{x=x_i^-}$, whereas the damaged region exhibits a reduced flexural stiffness, denoted as $EI_{x=x_i^+}$. Hence, the principle of force continuity can be employed to derive the following relationship:

$$EI_{x=x_i^-} \cdot \left.\frac{d^2w}{dx^2}\right|_{x=x_i^-} = EI_{x=x_i^+} \cdot \left.\frac{d^2w}{dx^2}\right|_{x=x_i^+} \tag{15}$$

$$\left.\frac{d^2w}{dx^2}\right|_{x=x_i^+} \Big/ \left.\frac{d^2w}{dx^2}\right|_{x=x_i^-} = EI_{x=x_i^-} \Big/ EI_{x=x_i^+} \tag{16}$$

Consequently, the ratio of the second derivative of flexural displacement across the damaged region's boundary exhibits an intrinsic correlation with the damage severity. Therefore, damage that can quantitatively alter the bending stiffness of the structure could be detected and measured. Taking the simplest case where damage is in the form of reduced thickness, we can deduce that

$$I_{x=x_i^+} = \frac{bh^3}{12}\left(1 - (1 - a/h)^3\right) \tag{17}$$

Substitute Eq. (17) into Eq. (16) yields

$$\mathrm{DSI} = a/h = 1 - \left(\left.\frac{d^2w}{dx^2}\right|_{x=x_i^-} \Big/ \left.\frac{d^2w}{dx^2}\right|_{x=x_i^+}\right)^{\frac{1}{3}} \tag{18}$$

where a is the slot-caused depth reduction; h is the height of the intact segment. It should be noted that, in principle, the LFC method can identify damages of various forms as long as they can alter the bending stiffness. The reduction of the cross-sectional area is considered here as a representative case. The left-hand side of Eq. (18) is defined as the Damage Severity Index (DSI) hereinafter, which indicates the relative damage severity. For damage with a non-uniform shape, the method can scan the affected area by recursively applying the assessment technique, allowing for the reconstruction of the damage profile. Section 3.5 will demonstrate this capability through illustrative examples. Note that transverse vibration displacements can be accurately measured using various sensor technologies.

This approach offers several advantages, such as being less dependent on the boundary conditions, structural complexity, the type and frequency of external excitation signals. Compared to the original PE approach, it does not require the measurement of additional parameters. Additionally, unlike the fourth derivatives used in the strong form of the PE method, the LFC method only involves the second derivatives, thus enabling reduced sensitivity and increased robustness to noise. It is noteworthy that the LFC method not only enables quantitative damage identification, but also provides a means to calculate the pseudo force within the framework of the PE method. According to Eq. (12), assuming that the damage is in the form of reduced thickness, when $x_i \le x \le x_j$, we have

$$\mathrm{DI} = \frac{Ebh^3}{12}\left(1 - (1 - \mathrm{DSI})^3\right)\frac{d^4W(x)}{dx^4} - \rho bh\omega^2 W(x)\mathrm{DSI} \tag{19}$$

where b is the thickness of the beam. Given that the principles of local dynamic equilibrium and internal force continuity are rooted in fundamental mechanical equilibrium which remains valid in higher-dimensional systems, the LFC method can be extended to more complex structures beyond the one-dimensional beams. As previously discussed, the successful implementation of the PE approach in higher-dimensional and structurally complex systems provides strong evidence for the feasibility of extending the LFC method to similar structural systems.

3. Numerical results

To verify the efficacy of the LFC method, we first numerically model a beam containing a predefined damage and assess whether the proposed approach can accurately detect the extent of the damage. Note such a model is for the sole purpose of providing simulated data to test the method, knowing that in practice, no global model is needed, and the structure can eventually be of arbitrary types as

long as the area under inspection is a beam component. The lumped-mass method and the finite element method are separately implemented to calculate the vibration response of the system. The displacement fields and their spatial derivatives are then processed to identify the positions and severity of damage by using the proposed LFC approach. The study then explores the influence of excitation frequency, damage location, and boundary conditions on the accuracy of damage severity identification. Finally, the LFC method is employed to achieve the inversion of the damage profile by identifying the DSI at each location within the damaged region.

3.1. Lumped mass method

The lumped mass method is employed to discretize continuous systems in this study. This section elucidates the modeling process using the lumped-mass method, taking the damaged Euler-Bernoulli beam as an illustrative example. First, the structure is discretized into discrete segments, with each segment specified as a nodal point where mass is concentrated. The mass and stiffness matrices of the undamaged structure are then constructed, assuming each segment has a uniform length Δx, with mass, stiffness, and damping concentrated as $m_i = \rho_0 A_0 \Delta x$, $k_i = E_0 I_0/(\Delta x)^3$, and $c_i = C\Delta x$ respectively. This leads to the dynamic equation governing these undamaged elements:

$$m_i\ddot{u} + c_i\dot{u} + k_i u = f_i(t) \tag{20}$$

where $\ddot{u}$, $\dot{u}$, u,and $f_i(t)$ donate acceleration, velocity, displacement, and external force at the $i-th$ node, respectively. Damage is introduced by assigning the $id-th$ element as the damaged element, with the corresponding mass, stiffness, and damping at each node changed to $m_{id} = \rho_d A_d \Delta x$, $k_{id} = E_d I_d/(\Delta x)^3$, and $c_{id} = C\Delta x$, where E_d, ρ_d, I_d, and A_d are the elastic modulus, density, moment of inertia, and cross-sectional area of the damaged element, respectively. The dynamic equation for the damaged element writes,

$$m_{id}\ddot{u} + c_{id}\dot{u} + k_{id}u = f_{id}(t) \tag{21}$$

With the governing equations for both damaged and undamaged elements established, the dynamic governing equation for the entire system can be formulated as

$$\mathbf{M}\ddot{\mathbf{u}} + \mathbf{C}\dot{\mathbf{u}} + \mathbf{K}\mathbf{u} = \mathbf{F}(t) \tag{22}$$

where $\mathbf{M}$, $\mathbf{C}$, $\mathbf{K}$, and $\mathbf{F}(t)$ are the mass, damping, stiffness, and external forces matrices, respectively, defined as

$$\mathbf{M} = \mathrm{diag}(m_1, m_2, \cdots, m_{id}, \cdots, m_n) \tag{23}$$

$$\mathbf{C} = \mathrm{diag}(c_1, c_2, \cdots, c_{id}, \cdots, c_n) \tag{24}$$

$$\mathbf{K} = \mathrm{tridiagonal}(-k_i, k_i + k_{i+1}, -k_{i+1}),\ i = 1 \sim id \sim n \tag{25}$$

$$\mathbf{F}(t) = (f_1(t), f_2(t), \cdots, f_{id}(t), \cdots, f_n(t)) \tag{26}$$

Finally, the displacement response of the entire damaged structures under vibrational loads can be solved through methods such as modal decomposition, the Newmark-β method, the Runge-Kutta method, and the Wilson-θ method.

A cantilever beam serves as a representative example. The beam (345 mm long, 19 mm wide and 6 mm thick; Young's modulus: $68.9\times(1+10^{-3}i)$ GPa; density: 2700 kg/m^3), is clamped at its left end and bears a through-width damaged zone from $x_d - d/2$ to $x_d + d/2$ along the beam axis (centralized at x_d with a length of d), as shown in Fig. 3. It is worth noting that due to its high aspect ratio ($l/h = 57.5$) and minor shear effects, the beam was modeled using Euler beam theory for simplicity. The whole beam is modeled

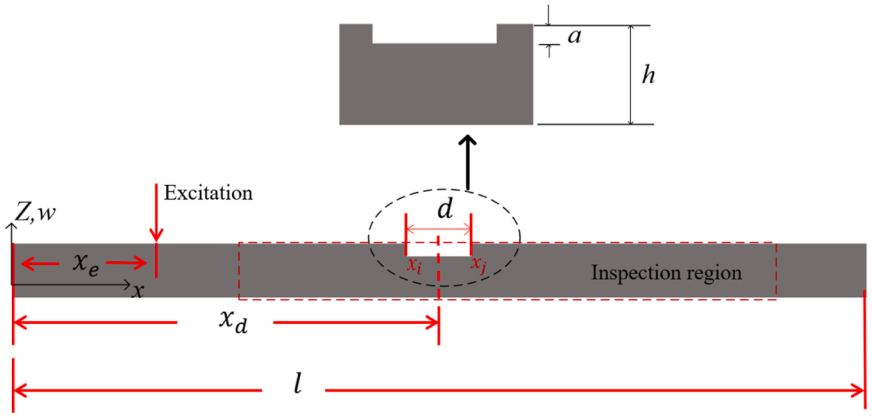

Fig. 3. Diagram of beam model.

with a total of 200 elements (1.725×10^{-3} m in length for each element). The damage is simulated with a reduction in beam thickness. $F(t)$ in Eq. (26) is set to a harmonic point force of frequency f at $x_e = 0.035$ m. To avoid any singularity (singular points in the DI caused by these external loads) near the excitation force, an inspection region ($L_{inspection} = 0.255$ m, starting at a distance of 0.07 m away from the left end) is selected by excluding the vicinity of x_e. Severity of the damage is defined by DSI $= a/h$. The above steps are implemented and solved utilizing MATLAB software.

3.2. Validations against finite element model

The lump-mass model is compared to the finite element model shown in Fig. 4, in term of vibration response for validation. In the latter case, the analysis is performed using COMSOL Multiphysics. The structural dimensions and material properties are the same as those used in the lumped mass method. A harmonic force with a unity amplitude is applied 35 mm from the fixed end of the beam in the transverse direction. Mesh convergence studies indicate that a maximum element size of 2 mm is enough to ensure simulation accuracy, resulting in about two thousand three-dimensional hexahedral solid elements discretizing the beam. The entire system is subject to a transverse excitation at a prescribed frequency, $F_0\delta(x+d)e^{i\omega t}$, which is exerted at 0.035 m from the origin ($x_e = 0.035$ m, $F_0 = 20$ N). Both eigenfrequency and frequency domain analyses are conducted, and displacement responses at the predefined inspection points are extracted to determine the damage location and severity according to Eq. (27) and Eq. (28).

3.3. Quantification of damage severity

A cantilever beam with a damaged zone spanning from $x_d - d/2$ to $x_d + d/2$ (x_d= 0.22 m, $d = 0.01$ m) is used as an example to verify the effectiveness of the LFC method using the two numerical modeling approaches as described above. The Frequency Response Function (FRF) of the beam at $x = 0.07$ m, and displacement fields of the beam considering the damage with DSI = 0.5 under excitation frequency of 60 Hz, obtained from both lumped mass and finite element modeling methods, are shown in Fig. 5(a) and (b), respectively. The near-identical displacement fields obtained from both methods validate the modeling accuracy of both approaches, confirming their consistency and reliability.

In the PE and LFC methods, the fourth and second derivatives of vibration displacement can be obtained through finite difference calculations. Assuming the displacement at the discrete point i is represented as w_i, the displacement values collected from adjacent points ranging from $i-2$ to $i+2$ allow for the computation of the fourth and second derivatives at point i. Therefore, DI and DSI can be formulated as:

$$\mathrm{DI}_i = E_0 I_0 \left(\frac{w_{i-2} - 4w_{i-1} + 6w_i - 4w_{i+1} + w_{i+2}}{d_m^4} \right) - \rho_0 A_0 \omega^2 w_i \tag{27}$$

$$\mathrm{DSI}_i = a/h = 1 - \left((w_{i-2} - 2w_{i-1} + w_i)/(w_{i-1} - 2w_i + w_{i+1}) \right)^{\frac{1}{3}} \tag{28}$$

In the calculation of high-order derivatives, measurement density would significantly affect the accuracy of the damage identification [38]. In theory, a denser distribution of measurement points allows for a more accurate detection of damage locations. However, the impact of measurement noise becomes increasingly magnified with higher-order derivatives, particularly in densely sampled data points. Therefore, as noted in previous work [28], an appropriate selection of the measurement points allows for striking a balance between the detection resolution and the noise immunity. The optimized choice, as suggested in [28], is to use approximately ten measurement points per wavelength when the fourth-order derivatives are involved. Due to the high accuracy of both the lumped mass method and the finite element method in solving the displacement field, the distribution of measurement points in this Section is set to 109 points per wavelength in the inspection region.

Fig. 6(a) and (b) illustrate the DI distributions derived from the displacement fields in Fig. 5 using Eq. (12). Pronounced oscillations at the damage boundary arise due to changes in the structural physical parameters upon reaching the damaged region, thus outlining the boundary of the damage. The DI values within the damage boundary quantify the magnitude of the pseudo force, reflecting the disturbance of the initial local equilibrium caused by the damage. This pseudo force is effectively equivalent to a nonexistent force

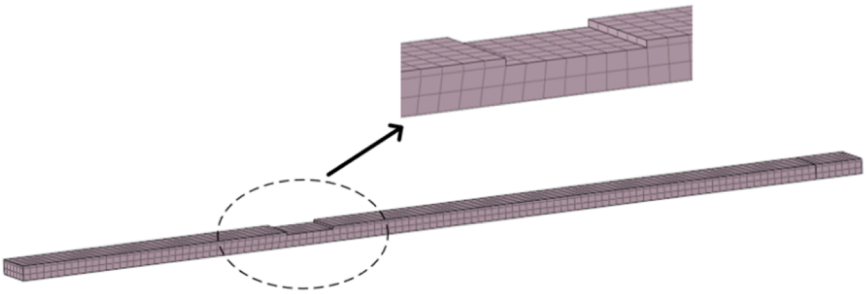

Fig. 4. Finite element model in COMSOL.

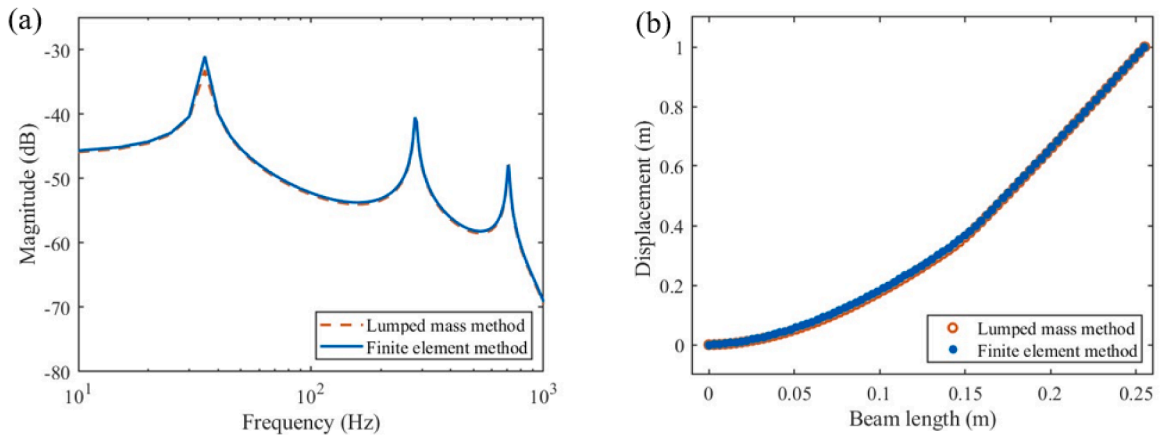

Fig. 5. Comparison of (a) FRF curves; and (b) displacement field between lumped mass method and finite element method.

acting on the original beam. The accuracy of the damage localization results indicates that the precision of the displacement field obtained through those two methods is sufficient to meet the requirements of the PE method for computing the fourth-order derivatives. Nevertheless, as observed in Fig. 6(b), minor oscillations are present within the damaged area. This is attributed to errors introduced during the finite element method's solution process. Although the displacement fields obtained by both methods exhibit satisfactory consistency, it is worth noting that the process of deriving the fourth-order derivative amplifies these errors, which aligns with the previously discussed issue of noise sensitivity associated with higher-order derivative operation.

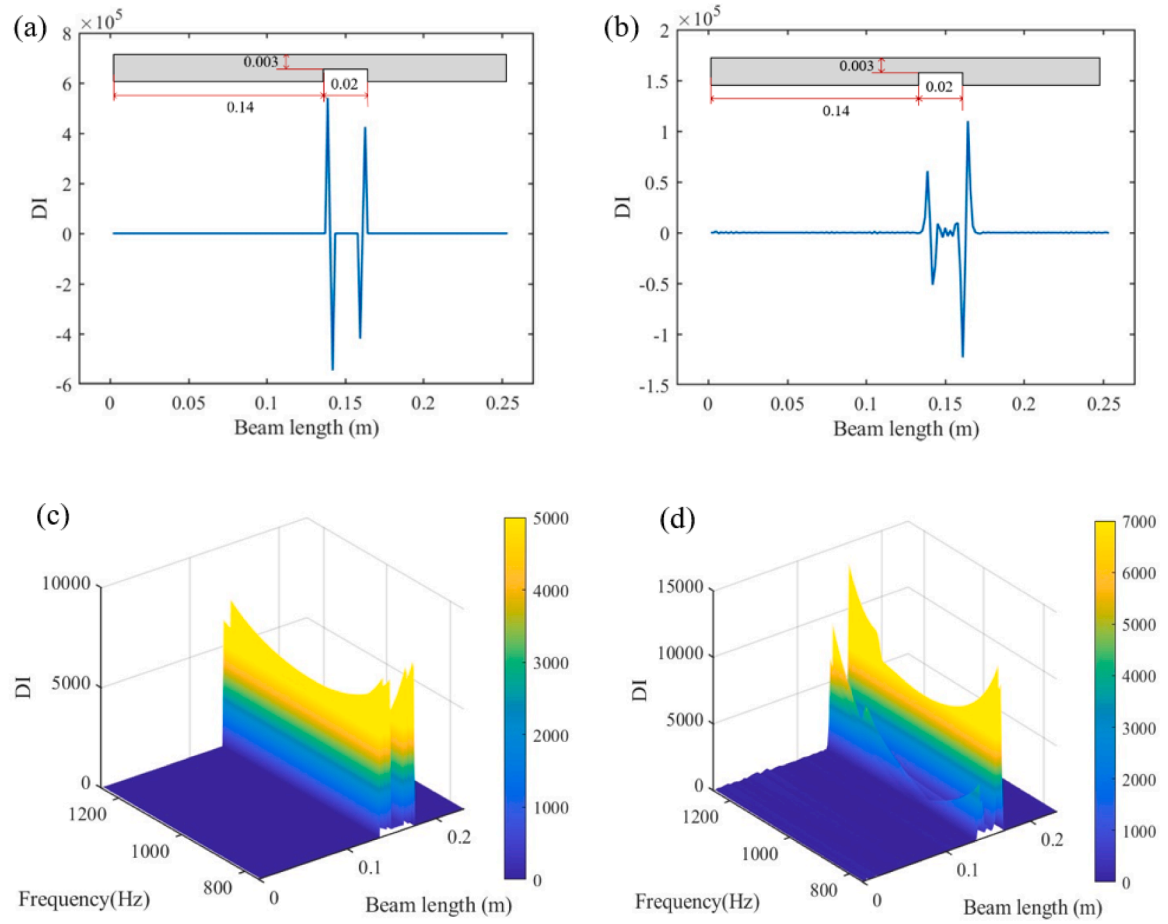

Fig. 6. Absolute value of DI at 60 Hz using (a) LM; (b) FEM and DI from 750Hz to 1250 Hz using (c) LM; (d) FEM.

To illustrate the applicability of the PE method across different frequencies, Fig. 6(c) and (d) present the curves of the absolute DI values within the 750-1250 Hz range. It is evident that, despite the frequency variations, the DI effectively indicates the actual damage locations, thus showing the independence of the proposed vibration-based local damage detection method on excitation frequency. In the most ideal scenario, each sinusoidal component under wideband excitation can be viewed as an independent detection channel, allowing for both damage quantification using a single frequency component or more comprehensive analysis by multi-frequency data fusion. A potential limitation of the proposed approach lies in compromised detection performance when damage occurs at modal nodes or when excitation is applied at nodal points. As demonstrated in Fig. 6(c) and (d), this limitation can be addressed through multi-frequency excitation and data fusion strategies, which provide complementary information and enhance detection robustness across the frequency spectrum.

Fig. 7 (a) and (b) show the DSI identification results within the damaged zone, obtained through the LFC method after pinpointing the location of the damage. The DSI values are effectively identified, with a maximum error of 0.04 and a relative error of 8%. As mentioned before, the LFC method not only entails quantitative damage identification, but also provides additional information about the pseudo force level. DI values in the damaged region represent a pseudo force. Once the DSI values are obtained, reverse inference can be applied to validate the concept of pseudo force using Eq. (19). As shown in Fig. 7 (c) and (d), the pseudo force derived from the identified DSI closely aligns with the distribution of the pseudo force defined by DI, with only minor discrepancies observed at certain peak values, which can be attributed to identification errors.

3.4. Quantification accuracy analysis

To evaluate the effectiveness of the LFC method in identifying varying DSI values, a comprehensive parametric analysis is conducted, with DSI ranging from 0.03 to 0.67 across 20 distinct parameter values. Additionally, DSI identification is performed under varying excitation frequencies, damage locations, and boundary conditions to systematically explore the impact of these factors on

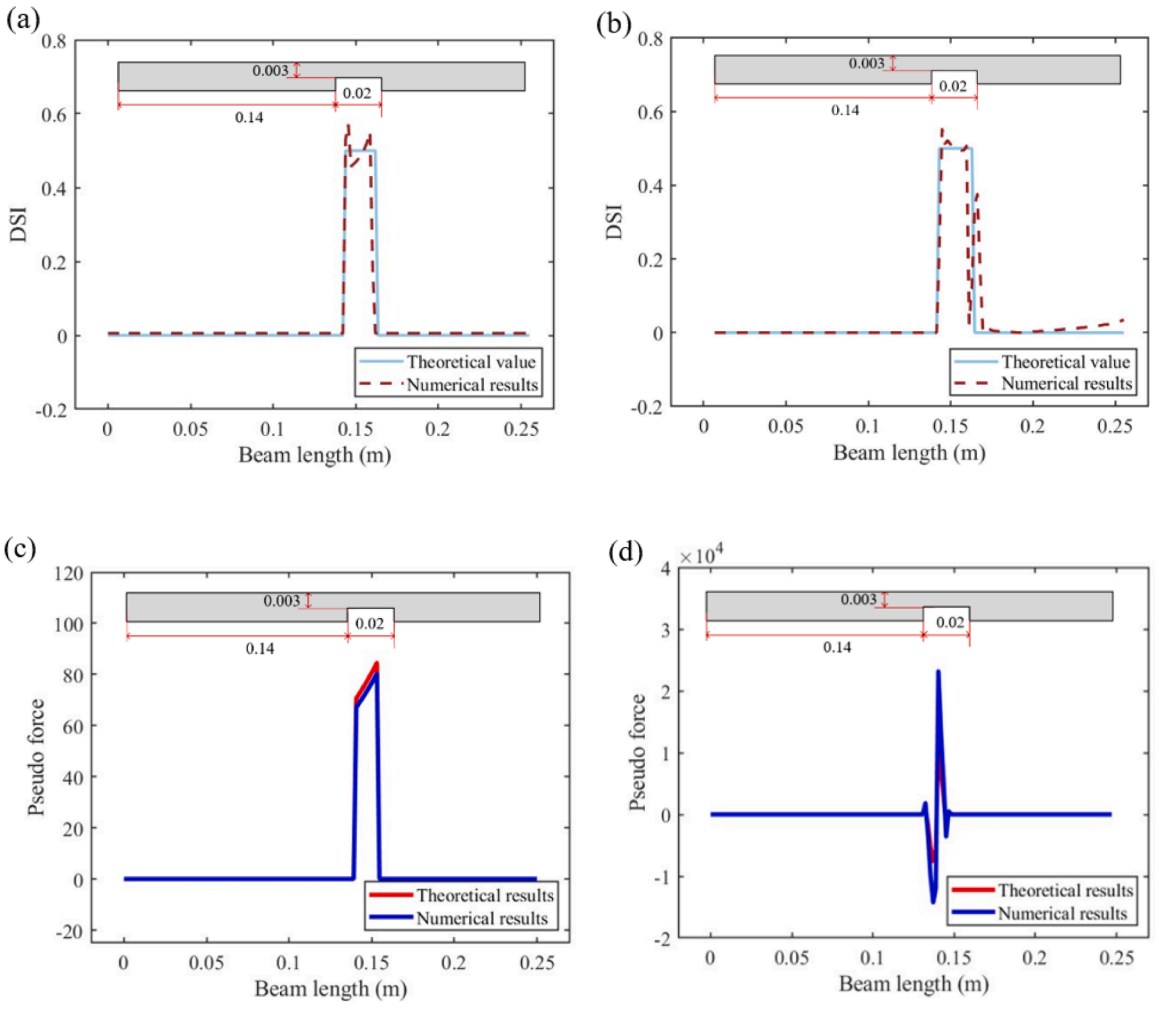

Fig. 7. DSI in (a) LM; (b) FEM; pseudo force in (c) LM; (d) FEM.

identification accuracy. Firstly, Fig. 8 examines the impact of excitation frequency on identification accuracy. Fig. 8(a) and (b) illustrate DSI values at frequencies of 50 Hz and 500 Hz, respectively. Apart from the excitation frequency and DSI variations, all other model parameters remain consistent with those outlined in Section 3.3. Fig. 8 illustrates that detection performance shows minor variations across different excitation frequencies. These variations do not arise from any intrinsic frequency dependence of the proposed method, which is theoretically effective across the entire frequency spectrum. Instead, such fluctuations are mainly attributed to the interplay between spatial sampling requirements and wavelength characteristics, as well as numerical challenges associated with higher-order derivative calculations—issues that merit further exploration in future research. The maximum error, e_{max}, is defined as the absolute ratio of the largest identified DSI error to the theoretical DSI value in each figure. The e_{max} for Fig. 8(a) and (b) are 12.7% and 14.5% respectively. The LFC method exhibits minimal identification errors for most DSI values across various frequencies, with even the largest errors remaining within an acceptable range.

Subsequently, the effectiveness of the LFC method in identifying DSI values for damage at different locations is assessed. Fig. 9(a) and (b) present the identification results for damage located at 0.04 m and 0.19 m, respectively, with e_{max} being 8.8% and 13.7%, indicating a high level of precision in damage detection across different locations. Furthermore, the investigation extends to examining the influence of boundary conditions on the accuracy of DSI identification by applying free-free and simply supported boundary conditions to the beam structure. This is depicted in Fig. 10(a) and (b), where the e_{max} are 10.1% and 15.7%, respectively. Different boundary conditions also lead to some slight variations in detection accuracy, indicating the need for more in-depth analysis in future studies.

In the field of damage detection based on global vibration signals, both traditional methods and machine learning techniques can be significantly influenced by excitation frequency, damage location, and boundary conditions. The proposed LFC method, as demonstrated in the above analyses, is almost immune to these varying factors and exhibits robust identification performance. This advantage stems from the inherent characteristics of the LFC method as a local damage detection approach, underpinned by solid physical principles. These research findings further corroborate that the LFC method is particularly suitable for precise damage quantification in complex structures under variable operating conditions. Although this study employs a simple beam structure for illustration, the LFC method actually possesses broad application potential and can be extended to more complex engineering practices.

3.5. Inversion of damage profile

Building upon the above, the proposed method can continuously reconstruct the damage profile by identifying the DSI at each point within the damaged region, using values derived from the previously identified data. In addition to uniform cross-sectional groove defects, this section also examines three different cross-sectional shapes: step-shaped, trapezoidal, and arc-shaped, to further expand the method's applicability. The dimensions of the structures containing these three types of defects are identical to those previously described, with the sole distinction being the shape and size of the defects. The specific dimensions of the defects are annotated in Figs. 11–13, respectively.

Fig. 11(a) and (b) illustrate the results of damage localization and quantitative analysis for step-shaped beam performed using the PE method and the LFC method, respectively. The PE method successfully identifies the location of the damage but fails to capture the extent of the damage within the affected region. In contrast, as evident from Fig. 11(b), the DSI curve clearly delineates the step-like defect shape. While notable oscillations are observed at locations where abrupt cross-sectional changes occur, the overall profile exhibits good agreement with the actual defect shape.

Figs. 12 and 13 present the geometric configurations and corresponding identification results for trapezoidal and arc-shaped defects, respectively. Although these figures clearly depict trapezoidal and arc-shaped DSI profiles, oscillatory behavior can be observed to the right of the damage region. The continuously changing profiles leads to computational errors caused by discrete sampling which cannot fully capture smooth transitions. Furthermore, the sequential nature of the LFC identification process causes errors at damage

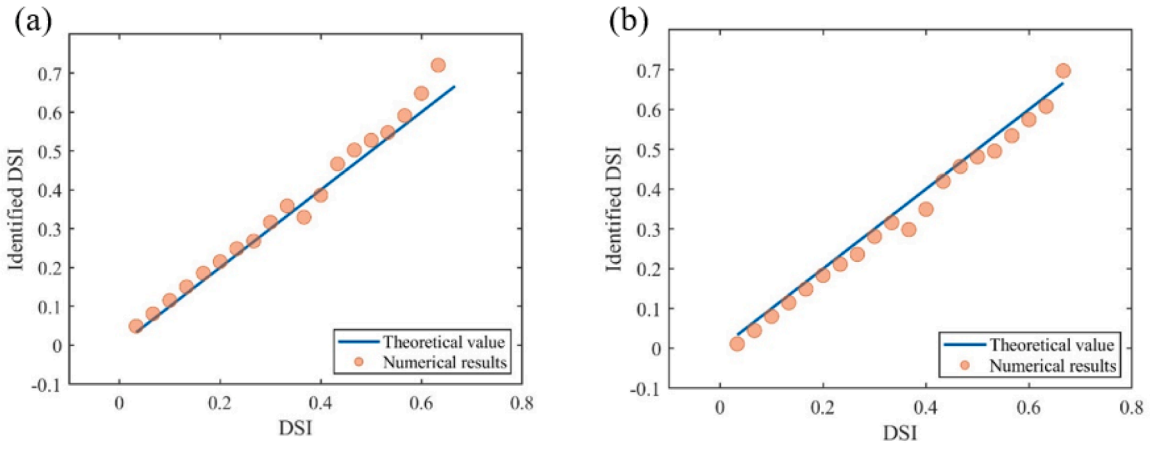

Fig. 8. Identified DSI under excitation frequency of (a) 50 Hz; (b) 500 Hz.

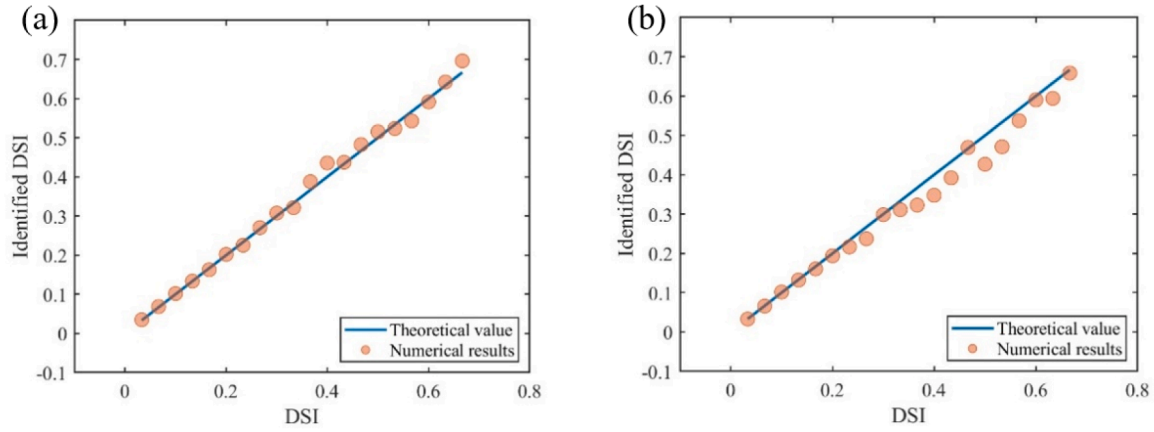

Fig. 9. Identified DSI when damage located at (a) 0.04 m; (b) 0.19m.

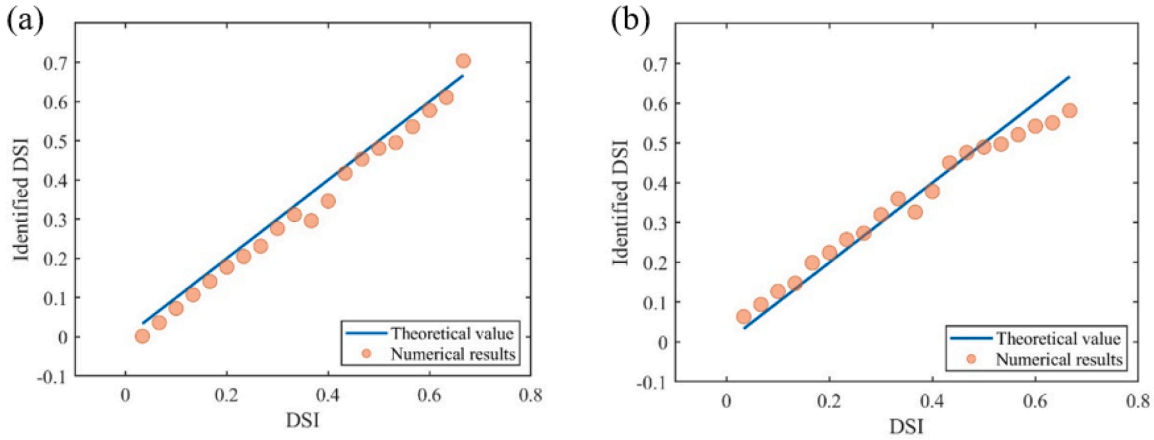

Fig. 10. Identified DSI under (a) free-free; (b) simply-supported.

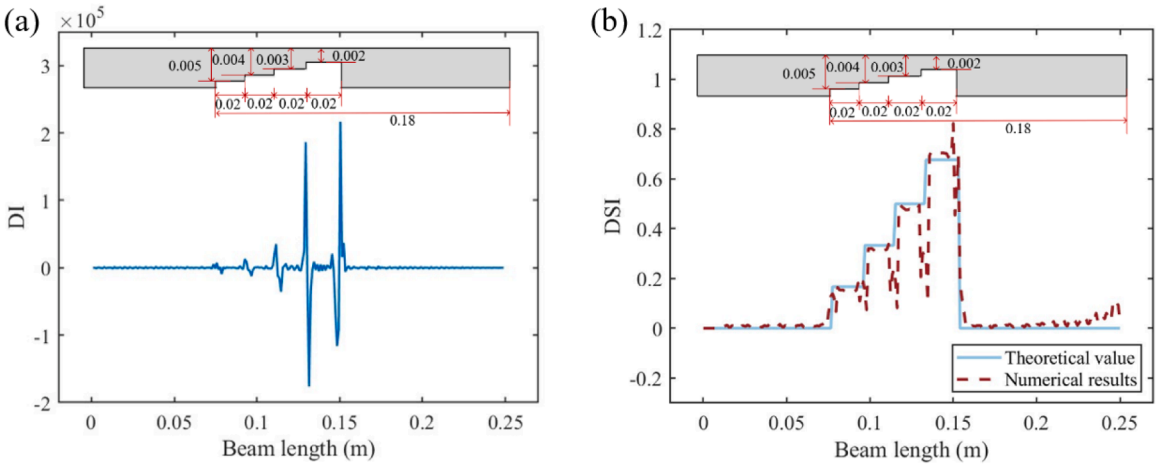

Fig. 11. (a) DI; and (b) Inversion of DSI of step-shaped beam.

boundaries to propagate to subsequent measurement points. This also explains the error observed in Fig. 13(b), where the maximum DSI occurs.

The aforementioned results indicate that, given a sufficient number of measurement points, the LFC method is capable of accurately

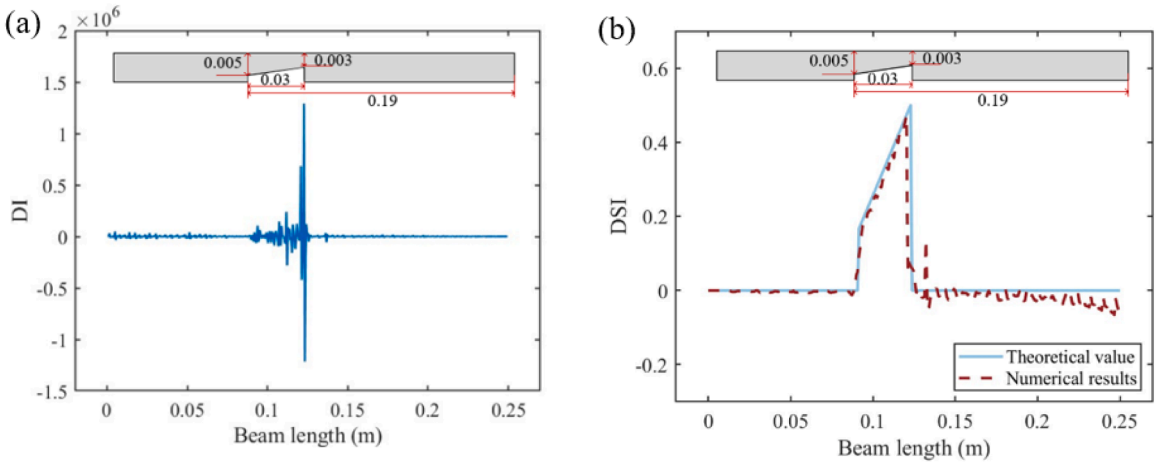

Fig. 12. (a) DI; and (b) Inversion of DSI of trapezoidal beam.

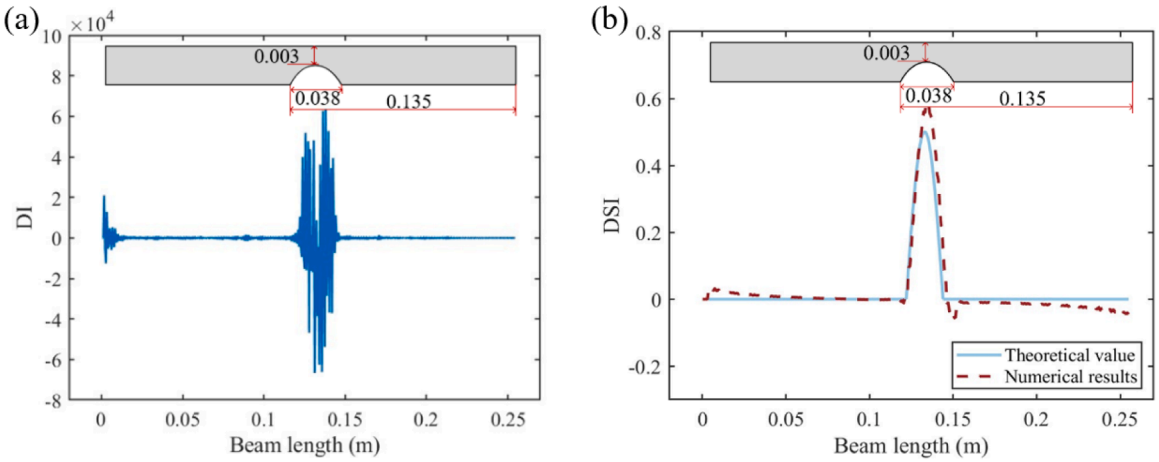

Fig. 13. (a) DI; and (b) Inversion of DSI of arc-shaped beam.

inverting damage profiles, even for continuously varying cross-sectional shapes. It is worth noting that the displacement fields are scanned on the intact side of the structure, alluding to the possibility of detecting internal defects behind it. Although defects that appear on the surface of the structure are studied here for better illustration, the LFC method is generally applicable to a wide range of defects, including internal ones inside the structure.

4. Experimental validations

This section presents an experimental validation of the proposed LFC method using a non-contact approach for damage identification in cantilever beam specimens. The efficacy of the method is demonstrated via localizing damage and quantifying DSI values across multiple test cases. Note again that this beam can represent a component within a more complex system that includes other structural elements, and it is worth noting that the proposed method is not constrained by the complexity of the structure, the boundary condition and the frequency of vibrational excitation.

4.1. Experimental setup

The experimental setup is schematically illustrated in Fig. 14. The beam is made of Al6061 aluminum alloy, with its material properties and geometric parameters tabulated in Table 1. Through-thickness notches of varying depths are precisely machined, positioned 0.21 m or 0.04 m from the fixed end of the beam. Five samples are shown in Fig. 15, where the damage profile is illustrated in the black rectangle. The dimensions of the samples, measured in meters, are presented alongside the corresponding results of damage identification. A harmonic excitation, generated using an electro-mechanical shaker (B&K 4089), is applied at 0.035 m from the fixed beam end. The inspection area measured 0.255 m in length is positioned 0.07 m away from the fixed end.

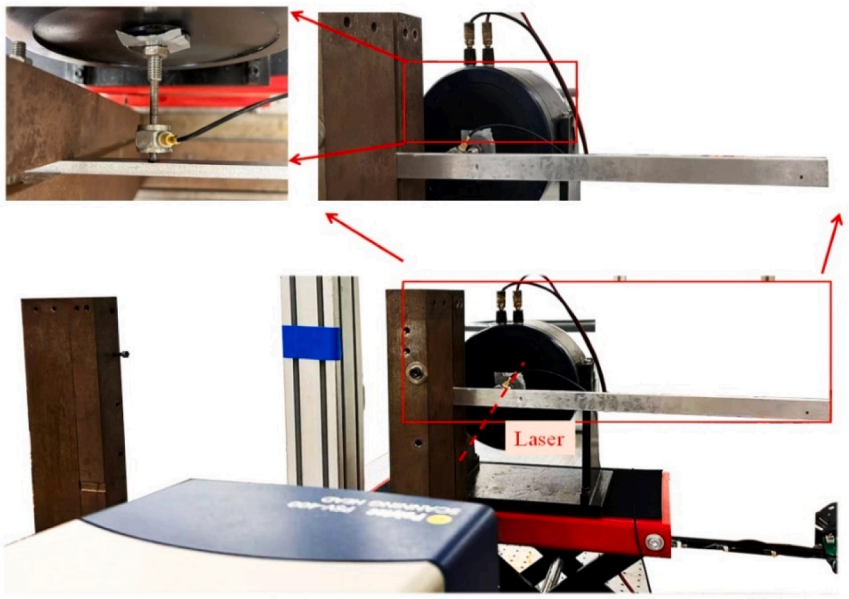

Fig. 14. Experimental setup.

The structural displacement is measured using a scanning Doppler laser vibrometer system (Polytec PSV-400). It should be noted that the effectiveness of the LFC method may be limited in environments where optical measurements cannot be performed. The experimental procedures are briefly outlined as follows:

Step 1: Setup the equipment and specimen

Install and position the Laser Doppler Vibrometer system and specimens at a suitable location.

Step 2: Configure the Measurement Region

An inspection region, slightly away from fixed boundaries and excitation points, is a priori selected. Measurement points are evenly distributed across the detection area, with a sampling density of about twenty points per wavelength, determined by the highest measurement frequency. A schematic illustration of the detection area and the distribution of measurement points is presented in in Fig. 16.

Step 3: Measure the vibration field

The damaged beam is excited using a B&K electromagnetic shaker. Sinusoidal frequency sweep ranging from 10 to 1000 Hz is generated as the input excitation signal. To obtain consistent results, vibration data at each measurement point are averaged over 30 acquisitions to reduce noise and measurement error.

Step 4: Data acquisition

Collect data at each measurement point to reconstruct the complete displacement field of the inspection region across the frequency range, check the quality of the acquired signals.

Step 5: Data processing

Substitute measured displacement field into DSI equation, i.e. Eq. (28), to identify the damage location and calculate the severity index.

Given the inevitability of measurement errors, we employ a sampling density of twenty measurement points per wavelength in the experimental phase. Although reference [28] suggests an optimal measurement density of ten points per wavelength, the LFC method's reliance solely on second-order derivatives of vibration displacement, rather than fourth-order derivatives, renders it less susceptible

Table 1
Material properties and geometric parameters of the beam used for experimental validation.

Density (kg/m^3)	2700
Young's Modulus E (GPa)	68.9
Beam length L (m)	0.365
Fixed length L_d (m)	0.02
Width b (m)	0.019
Thickness h (m)	0.006
Location of the excitation x_e (m)	0.035
Length of inspection region $L_{Inspection}$ (m)	0.255
Central location of damaged zone x_d (m)	0.21
Length of the damaged zone d (m)	0.02

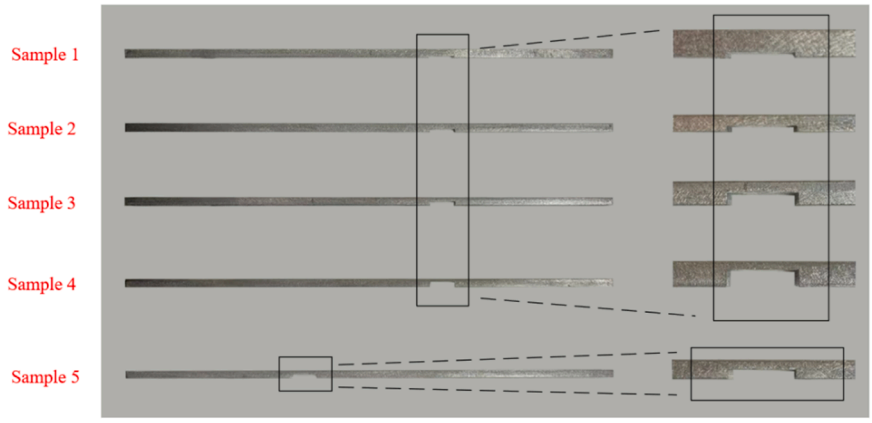

Fig. 15. Samples showing the shape of the damages to be identified using the proposed approach.

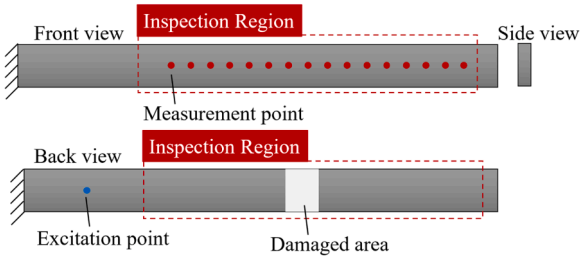

Fig. 16. A schematic illustration of the detecting area and measurement points distribution.

to error propagation. To minimize the potential influence of experimental errors that could lead to false damage identification, a two-stage strategy is adopted: first, the damage is roughly located using the DI, followed by a focused quantitative assessment within the identified damaged region using DSI. Zero DSI values were assigned to regions outside the damage zone, as these areas away from damages were not of primary interest.

This experiment was designed to validate the effectiveness of the proposed method in quantitatively describing damage severity, as well as to assess its robustness against variations in excitation frequency and damage location.

4.2. Results and discussions

To verify the reliability of the experimental data, a frequency sweep excitation is first applied to the beam, and the FRF curve is extracted at a specific point (70 mm from the fixed end) on the beam. The corresponding FRF curve is also obtained from the same location in the finite element model for comparison, as shown in Fig. 17 (a). Following this, as shown in Fig. 17 (b), the displacement field at 625 Hz obtained from the experiment is compared with that from the finite element model, exhibiting good agreement.

The constructed DI and DSI distribution in the inspection region for damage Samples 1, 2, 3, and 4 are presented in Fig. 18. The results indicate that the DI distribution obtained using the PE method exhibits significant oscillations at the location of the damage. Subsequently, the DSI values within the damaged region are identified using the LFC method, demonstrating that the LFC method provides effective identification across varying damage depths.

It can be seen that while numerical simulations demonstrate the method's high sensitivity to small stiffness variations, the above experimental results indicate that the practical detection limit of the LFC method is primarily governed by the signal-to-noise ratio of the measurement system. Fig. 19(a) and (b) illustrate the impact of excitation frequency and damage location on the identification accuracy. The results of the LFC method are found to be independent of both the excitation frequency and damage location, indicating their negligible influence on the identification results.

Table 2 presents the experimentally identified DSI values (the average DSI value within damage region) and their corresponding relative errors for Samples 1 through 5. The observed deviations fall within an acceptable range, with the minor discrepancies primarily attributable to measurement noise and the inherent challenges associated with numerical differentiation. These results demonstrate the robustness of the method in the presence of experimental uncertainties. When benchmarked against existing methods, the proposed LFC approach demonstrates comparable or superior performance in terms of accuracy. For example, Loutridis et al. [39] investigated the fundamental vibration mode of double-cracked beams using wavelet transform. In their study, when the actual DSIs were 20% and 30%, the identified DSIs were 30% and 40%, respectively, resulting in relative errors of 50% and 33.3%. Chen et al. [40] examined an aluminum beam with deflection influence lines. In their experiments, for a single crack damage with an actual DSI of

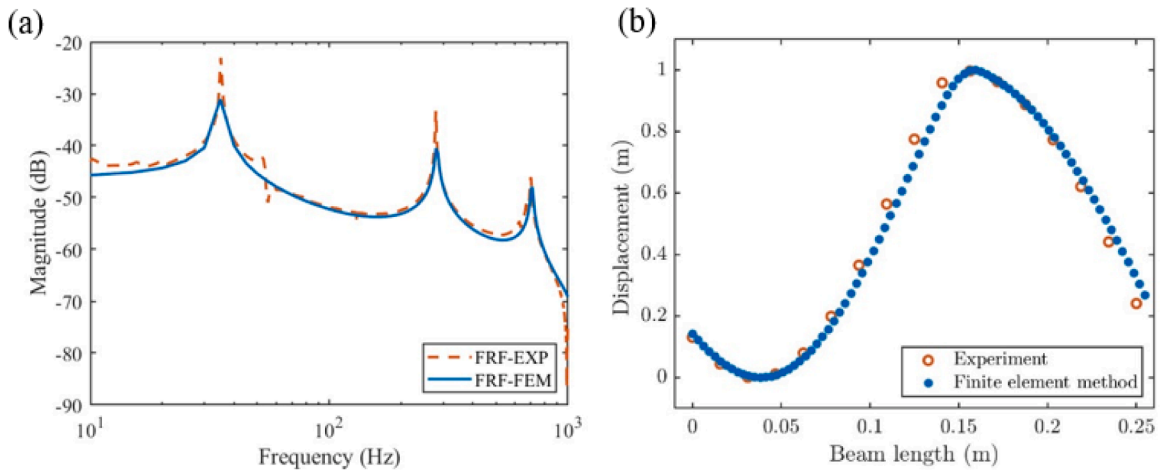

Fig. 17. Comparison of (a) FRFcurve; (b) displacement field between finite element and experimental data.

55%, the identified DSI was approximately 50% using a single sensor at midspan, leading to a relative error of 9.1%. Therefore, the proposed LFC method not only exhibits superior detection accuracy, but also offers several inherent advantages owing to its local, multi-frequency vibration-based and dynamic-enabled detection ability.

It should be noted that the current experiment examines a damage of finite length, where a reduction in local bending stiffness clearly creates discontinuities in the second derivatives at the damage boundaries. If the notch length approaches zero, the two boundaries merge into a single interface, resembling a crack. In such cases, the local structural stiffness at the interface may exhibit complicated behaviors. Future studies are needed to extend this method to address other types of damages and more complex structural configurations. Concerning minimum notch dimensions, the LFC method can theoretically detect any thickness reduction affecting bending stiffness. However, measurement noise and numerical errors in derivative calculations can impact accuracy, as illustrated in Figs. 18-19. Consequently, we anticipate that lower DSI values will make damage localization more challenging, compromising the accuracy of quantitative assessments. Therefore, the sensitivity of this approach should be carefully evaluated in practical applications.

5. Conclusions

This study presents a novel method for locating and quantifying damage severity contained in a structure based on the local force continuity conditions. Based on the continuity relationship that governs the local internal forces, this method effectively detects damage regions of finite width and is theoretically sensitive to any reduction in thickness, which represents a form of stiffness degradation. By examining variations in the spatial derivatives of vibration displacement, the severity of damage is the target of the inspection. Numerical simulations using both the lumped mass method and finite element method demonstrate that the proposed approach can reliably identify local damage depth, independent of excitation frequency, damage location, and boundary conditions. Also, by continuously tracking the identified local DSI, the method enables precise reconstruction of the damage profile. At the same time, effectiveness of the approach is experimentally examined by quantifying damage depth in a beam using a scanning laser vibrometer. Compared to the numerical results, the experimentally obtained damage depth predictions exhibit slightly larger errors, which can be attributed to measurement noise and the use of higher-order derivatives in the method. Overall, the experimental results confirm the effectiveness of the proposed approach.

As a local damage quantification method, LFC approach inherits all the advantages of the PE method, including the ability to operate without requiring vibration signals from an undamaged reference structure, no dependence on precise knowledge on global structural models, boundary conditions or excitation frequency, and no limitations regarding damage location or quantity. Furthermore, this method validates the concept of the pseudo force introduced in the PE method, advancing the method from mere damage localization to damage quantification without the need for additional data. Additionally, due to its localized nature, this method also enables the reconstruction of the shape of the damage, which is of significant importance for engineering applications.

It is noteworthy that the proposed method is inherently extensible from simple beam models to more complex engineering structures, since it is built on fundamental equilibrium principles applicable to higher-dimensional continuous bodies. With the ongoing development of measurement technologies, optical fiber-based sensing techniques and video-based image processing methods will greatly simplify the acquisition of vibration data and may further enhance the capabilities of the proposed method. Although measurement noise inevitably introduces errors in practical implementations, such effects can be effectively reduced through appropriate signal-processing techniques and measurement strategies, thereby ensuring reliable performance in realistic scenarios.

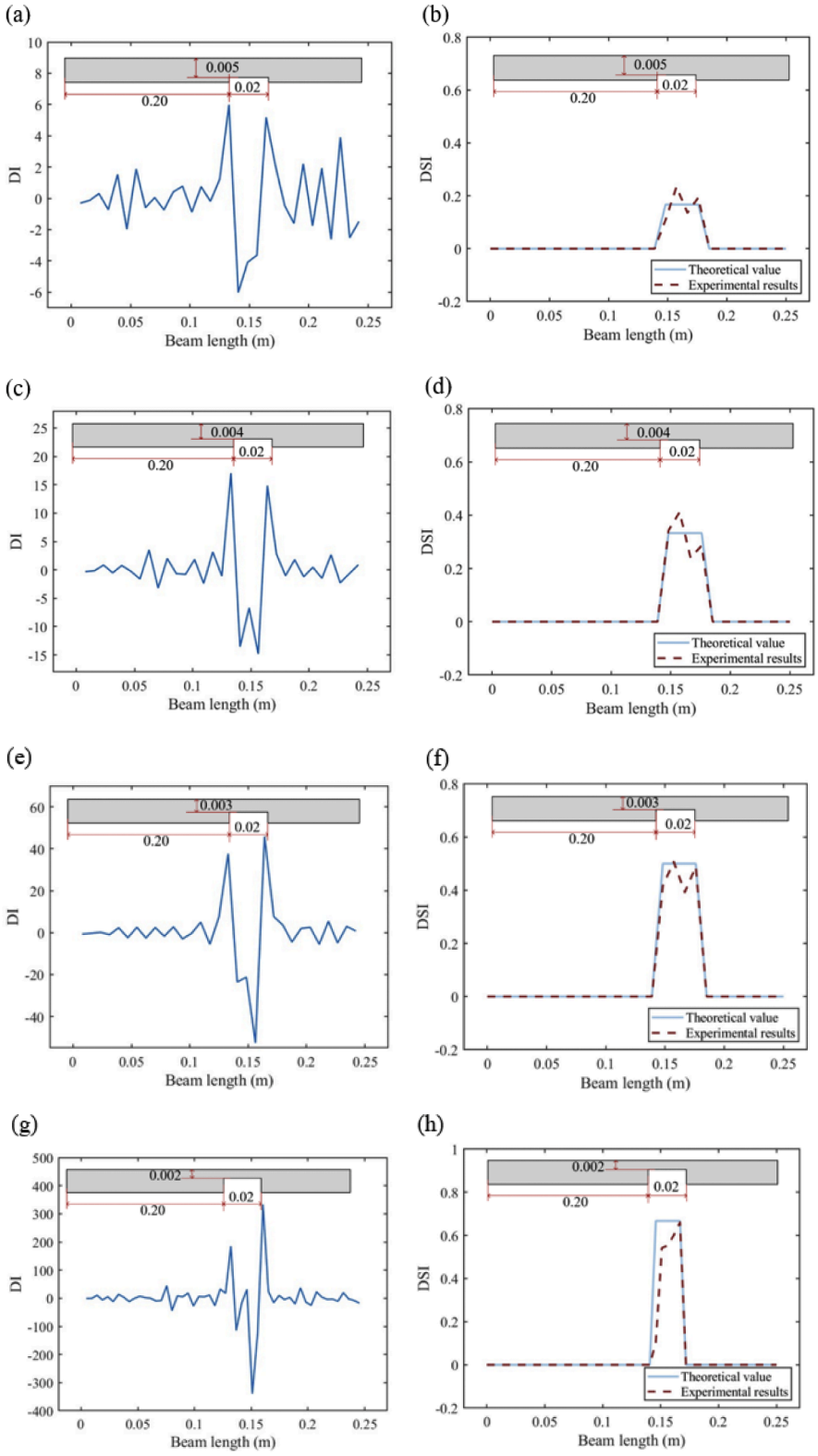

Fig. 18. Experimentally identified damage extents of samples: (a) & (b) DI and DSI of sample 1; (c) & (d) DI and DSI of sample 2; (e) & (f) DI and DSI of sample 3; (g) & (h) DI and DSI of sample 4.

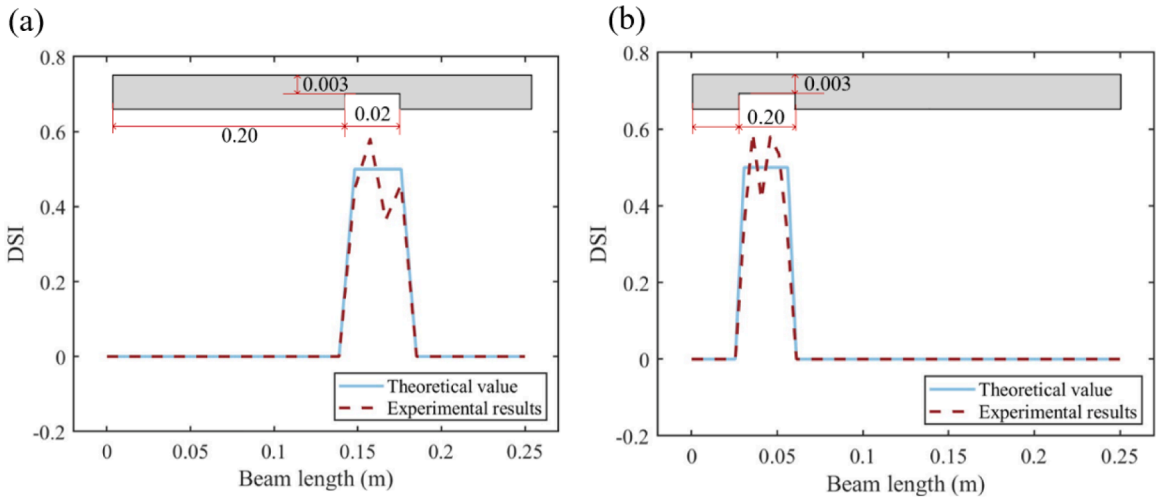

Fig. 19. DSI of (a) sample with damage location of 0.21 m at 600 Hz; (b) sample with damage location of 0.04 m at 240 Hz.

Table 2
Relative errors of experimental identification values.

Samples	Expected DSI	Identified DSI	Errors
1	0.167	0.171	-2.39%
2	0.333	0.391	17.42%
3	0.500	0.418	-16.4%
4	0.667	0.602	9.75%
5	0.500	0.485	-8.40%

CRediT authorship contribution statement

Yuting Yang: Writing – original draft, Validation, Methodology, Investigation. **Yu'e Ma:** Writing – review & editing, Supervision. **Linfeng Li:** Writing – review & editing, Validation. **Li Cheng:** Writing – review & editing, Supervision, Methodology. **Xiang Yu:** Writing – review & editing, Validation, Supervision, Methodology.

Declaration of competing interest

The authors declare that they have no known competing financial interests or personal relationships that could have appeared to influence the work reported in this paper.

Acknowledgements

This research was supported by the National Natural Science Foundation of China (Grant No. U2341238) and the Research Institute for Artificial Intelligence of Things (RIAIoT) of the Hong Kong Polytechnic University. The authors also acknowledge the support from the PolyU Dual Degree Research Postgraduate Scholarship.

Data availability

Data will be made available on request.

References

[1] C. Zhang, H. Xu, Z. Su, L. Cheng, Damage detection based on sparse virtual element boundary measurement using metal-core piezoelectric fiber, Struct. Health Monit. 17 (2018) 15–23, https://doi.org/10.1177/1475921717735574.
[2] Z. Pan, T. Liu, J. Zhang, H. Wang, F. Sun, W. Li, A two-stage method based on extreme learning machine for predicting the remaining useful life of rolling-element bearings, Mech. Syst. Signal Process. 144 (2020) 106899, https://doi.org/10.1016/j.ymssp.2020.106899.
[3] S. Zhu, J. Huang, H. Peng, D. Yin, C. Lu, Fatigue reliability assessment of turbine discs under multi-source uncertainties, Fatigue Fract. Eng. Mater. Struct. 41 (2018) 1291–1305, https://doi.org/10.1111/ffe.12773.
[4] C. Liu, J.B. Harley, M. Bergés, D.W. Greve, I.J. Oppenheim, Robust ultrasonic damage detection under complex environmental conditions using singular value decomposition, Ultrasonics 58 (2015) 75–86, https://doi.org/10.1016/j.ultras.2014.12.005.

[5] N. Tao, A.G. Anisimov, R.M. Groves, Shearography non-destructive testing of thick GFRP laminates: numerical and experimental study on defect detection with thermal loading, Compos. Struct. 282 (2022) 115008, https://doi.org/10.1016/j.compstruct.2021.115008.
[6] P. Cotič, D. Kolarič, V.B. Bosiljkov, V. Bosiljkov, Z. Jagličić, Image fusion for improved detection of near-surface defects in NDT-CE using unsupervised clustering methods, J. Nondestruct. Eval. 33 (2014) 384–397, https://doi.org/10.1007/s10921-014-0238-8.
[7] A. Zarei, S. Pilla, Laser ultrasonics for nondestructive testing of composite materials and structures: a review, Ultrasonics 133 (2023) 107163, https://doi.org/10.1016/j.ultras.2023.107163.
[8] Y.H. Yu, J.H. Choi, J.H. Kweon, D.H. Kim, A study on the failure detection of composite materials using an acoustic emission, Compos. Struct. 75 (2006) 163–169, https://doi.org/10.1016/j.compstruct.2006.04.032.
[9] O. Avci, O. Abdeljaber, S. Kiranyaz, M. Hussein, D.J. Inman, A review of vibration-based damage detection in civil structures: from traditional methods to machine learning and deep learning applications, Mech. Syst. Signal Process. 147 (2021) 107077, https://doi.org/10.1016/j.ymssp.2020.107077.
[10] W. Fan, P. Qiao, Vibration-based damage identification methods: a review and comparative study, Struct. Health Monit. 10 (2011) 83–111, https://doi.org/10.1177/1475921710365419.
[11] K. Skowronek, M. Bocian, J. Bień, T. Kalisch, Assessment of background noise properties in time and time–frequency domains in the context of vibration-based local damage detection in real environment, Mech. Syst. Signal Process. 199 (2023) 110465, https://doi.org/10.1016/j.ymssp.2023.110465.
[12] H.W. Shih, D. Thambiratnam, T. Chan, Vibration based structural damage detection in flexural members using multi-criteria approach, J. Sound Vib. 323 (2009) 645–661, https://doi.org/10.1016/j.jsv.2009.01.019.
[13] Y. Xia, H. Hao, Statistical damage identification of structures with frequency changes, J. Sound Vib. 263 (2003) 853–870, https://doi.org/10.1016/S0022-460X(02)01077-5.
[14] N. Maia, J.M.M. Silva, E.A.M. Almas, R.P.C. Sampaio, Damage detection in structures: from mode shape to frequency response function methods, Mech. Syst. Signal Process. 17 (2003) 489–498, https://doi.org/10.1006/mssp.2002.1506.
[15] A. Alvandi, C. Cremona, Assessment of vibration-based damage identification techniques, J. Sound Vib. 292 (2006) 179–202, https://doi.org/10.1016/j.jsv.2005.07.036.
[16] J. Humar, A. Bagchi, H. Xu, Performance of vibration-based techniques for the identification of structural damage, Struct. Health Monit. 5 (2006) 215–241, https://doi.org/10.1177/1475921706058809.
[17] C.P. Ratcliffe, Damage detection using a modified Laplacian operator on mode shape data, J. Sound Vib. 204 (1997) 505–517, https://doi.org/10.1006/jsvi.1997.0961.
[18] D. Dessi, G. Camerlengo, Damage identification techniques via modal curvature analysis: overview and comparison, Mech. Syst. Signal Process. 52 (2015) 181–205, https://doi.org/10.1016/j.ymssp.2014.07.004.
[19] J. Ciambella, A. Pau, F. Vestroni, Modal curvature-based damage localization in weakly damaged continuous beams, Mech. Syst. Signal Process. 121 (2019) 171–182, https://doi.org/10.1016/j.ymssp.2018.11.012.
[20] C.C. Chang, L.W. Chen, Damage detection of cracked thick rotating blades by a spatial wavelet based approach, Appl. Acoust. 65 (2004) 1095–1111, https://doi.org/10.1016/j.apacoust.2004.04.006.
[21] M. Djamaa, N. Ouelaa, C. Pezerat, J.L. Guyader, Reconstruction of a distributed force applied on a thin cylindrical shell by an inverse method and spatial filtering, J. Sound Vib. 301 (2007) 560–575, https://doi.org/10.1016/j.jsv.2006.10.023.
[22] T. Zhang, Y. Xu, Z. Liu, X. Wang, H. Li, Vibration-based structural damage detection via phase-based motion estimation using convolutional neural networks, Mech. Syst. Signal Process. 178 (2022) 109320, https://doi.org/10.1016/j.ymssp.2022.109320.
[23] R. Ghiasi, P. Torkzadeh, M. Noori, A machine-learning approach for structural damage detection using least square support vector machine based on a new combinational kernel function, Struct. Health Monit. 15 (2016) 302–316, https://doi.org/10.1177/1475921716639587.
[24] H.B. Bisheh, G.G. Amiri, Structural damage detection based on variational mode decomposition and kernel PCA-based support vector machine, Eng. Struct. 278 (2023) 115565, https://doi.org/10.1016/j.engstruct.2022.115565.
[25] Z. Nie, H. Ma, Z. Wei, X. Wang, Baseline-free structural damage detection using PCA-Hilbert transform with limited sensors, J. Sound Vib. 568 (2024) 117966, https://doi.org/10.1016/j.jsv.2023.117966.
[26] Y. Bao, Y. Guo, H. Li, A machine learning–based approach for adaptive sparse time–frequency analysis used in structural health monitoring, Struct. Health Monit. 19 (2020) 1963–1975, https://doi.org/10.1177/1475921719900918.
[27] M. Makki Alamdari, B. Samali, J. Li, Y. Lu, S. Mustapha, Frequency domain decomposition-based multisensor data fusion for assessment of progressive damage in structures, Struct, Control Health Monit. 26 (2019) e2299, https://doi.org/10.1002/stc.2299.
[28] H. Xu, L.Z. Su, M.S. Cao, Y. Xia, Identification of structural damage based on locally perturbed dynamic equilibrium with an application to beam component, J. Sound Vib. 330 (2011) 5963–5981, https://doi.org/10.1016/j.jsv.2011.07.020.
[29] M. Cao, W. Xu, W. Ostachowicz, Z. Su, A multi-scale pseudo-force model in wavelet domain for identification of damage in structural components, Mech. Syst. Signal Process. 28 (2012) 638–659, https://doi.org/10.1016/j.ymssp.2011.09.029.
[30] H. Xu, L. Cheng, Z. Su, M. Cao, Damage visualization based on local dynamic perturbation: theory and application to characterization of multi-damage in a plane structure, J. Sound Vib. 332 (2013) 3438–3462, https://doi.org/10.1016/j.jsv.2012.10.036.
[31] H. Xu, L. Cheng, Z. Su, M.S. Cao, Reconstructing interfacial force distribution for identification of multi-debonding in steel-reinforced concrete structures using noncontact laser vibrometry, Struct. Health Monit. 12 (2013) 507–521, https://doi.org/10.1177/1475921713500514.
[32] C. Zhang, H. Xu, L. Cheng, Z. Su, Structural damage detections based on a general vibration model identification approach, Mech. Syst. Signal Process. 123 (2019) 316–332, https://doi.org/10.1016/j.ymssp.2019.01.019.
[33] M. Cao, Z. Su, W. Xu, L. Cheng, A novel damage characterization approach for laminated composites in the absence of material and structural information, Mech. Syst. Signal Process. 143 (2020) 106831, https://doi.org/10.1016/j.ymssp.2020.106831.
[34] W. Xu, M. Cao, Q. Ding, M. Radzieński, W. Ostachowicz, A novel structural damage identification approach using damage-induced perturbation in longitudinal vibration, J. Sound Vib. 496 (2021) 115932, https://doi.org/10.1016/j.jsv.2021.115932.
[35] W. Xu, M. Cao, Y. Pan, W. Ostachowicz, Reconstruction of radial pseudo-forces on cylinders via mono-laser scanning: concept and application to characterization of damage, Mech. Syst. Signal Process. 200 (2023) 110570, https://doi.org/10.1016/j.ymssp.2023.110570.
[36] C. Zhang, H. Xu, Z. Su, L. Cheng, Structural damage detection based on virtual element boundary measurement, J. Sound Vib. 372 (2016) 133–146, https://doi.org/10.1016/j.jsv.2016.02.029.
[37] C. Zhang, H. Xu, Z. Su, L. Cheng, Damage detection based on sparse virtual element boundary measurement using metal-core piezoelectric fiber, Struct. Health Monit. 17 (2018) 15–23, https://doi.org/10.1177/1475921717735574.
[38] E. Lofrano, et al., Optimal sensors placement in dynamic damage detection of beams using a statistical approach, J. Optim. Theory Appl. 187 (2020) 758–775, https://doi.org/10.1007/s10957-020-01761-3.
[39] S. Loutridis, E. Douka, A. Trochidis, Crack identification in double-cracked beams using wavelet analysis, J. Sound Vib. 277 (2004) 1025–1039, https://doi.org/10.1016/j.jsv.2003.09.035.
[40] Z.W. Chen, Q.L. Cai, S. Zhu, Damage quantification of beam structures using deflection influence lines, Struct. Control Health Monit. 25 (2018) e2242, https://doi.org/10.1002/stc.2242.